Front. Chem. China 2010, 5(4): 435–444
DOI 10.1007/s11458-010-0220-7

REVIEW ARTICLE

Probing polymer surfaces and interfaces using sum frequency generation vibrational spectroscopy – a powerful nonlinear optical technique

Xiaolin LU (✉)[1], Zhan CHEN[2], Gi XUE (✉)[3] and Xinping WANG[1]

Sum frequency generation (SFG) vibrational spectroscopy has been proved to be a powerful technique which substantially impacts on many research areas in surface and interfacial sciences. This paper reviews the recent progress of applying this nonlinear optical technique in the studies of polymer surfaces and interfaces. The theoretical background of SFG is introduced first. Current applications of SFG in polymer science are then described in more detail to demonstrate the significance of this technique. Finally, a short summary is presented on this relatively new but widely applicable spectroscopic technique.

Keywords sum frequency generation vibrational spectroscopy, SFG, nonlinear optical technique, surface and interface, polymer

1 Introduction

Polymer is one of the most widely used materials, with a variety of applications in coatings, biomedical implants, microelectronic devices, and composites etc. In these applications, the polymer surface and/or interfacial properties are extremely important. These properties are determined by the molecular structures of the surface or interface. Therefore in order to optimize the surface/interfacial properties in these applications, it is necessary to fully understand the polymer surface/interfacial structure-property relationships, after characterizing the polymer surface and interfacial molecular structures. Many surface-sensitive techniques have been developed in the past several decades, including the attenuated total reflection infrared spectroscopy (ATR-IR) [1,2], surface enhanced Raman scattering (SERS) [3,4], X-ray photoelectron spectroscopy (XPS) [5–7], secondary ion mass spectroscopy (SIMS) [6,7], and near edge X-ray absorption fine structure (NEXAFS) spectroscopy [8,9], etc. Even though excellent research results have been reported by using these techniques in the studies, each technique has some weaknesses in surface/interface characterizations. Some of the above techniques lack the desired surface sensitivity (e.g., ATR-IR), while others need a high-vacuum environment to operate, which prevents the in situ characterization (e.g., XPS, SIMS, and NEXAFS). SERS requires special metal surfaces or particles to enhance the signal, which cannot be applied to investigate many different surfaces or interfaces.

In the last twenty years, a second-order nonlinear optical spectroscopy, sum frequency generation (SFG) vibrational spectroscopy has been developed into a powerful technique to probe the molecular structures of various surfaces and interfaces in situ. The first SFG paper was published in 1987, examining the adsorption of methanol and pentadecanoic acid monolayers on the glass and water [10]. After that, tremendous progress has been made in the development of SFG theoretical description, instrumentation, data analysis, and applications [11–26]. Nowadays SFG becomes a widely used technique by a large number of research groups to study polymer surfaces and interfaces, catalysis, biochemical processes, self-assembled monolayers, and small molecular liquids, ionic liquids, water structures on surfaces and at interfaces. SFG is a nonlinear optical technique and a molecular vibrational spectroscopy. Therefore scientists carrying out SFG research are required to have some background knowledge in nonlinear optics and molecular spectroscopy. Fortunately, there have already been excellent books/review articles introducing such background knowledge. This paper is a general introduction of SFG vibrational spectroscopy using concise language (hopefully without losing its essence), emphasizing on practical applications of the technique in polymer studies. The recent advances of SFG studies on the molecular structures of polymer surfaces and interfaces are presented. For more detailed understanding, readers are strongly recommended to look into many SFG review articles [13–26].

2 Theoretical background

As a second-order nonlinear optical technique, an SFG process involves two incoming photons and one output

Received July 13, 2010; accepted September 18, 2010
1. Department of Chemistry, Key Laboratory of Advanced Textile Materials and Manufacturing Technology of Education Ministry, Zhejiang Sci-Tech University, Hangzhou 310018, China
2. Department of Chemistry, University of Michigan, 930 North University Avenue, Ann Arbor, Michigan 48109, USA
3. Department of Polymer Science, Nanjing University, Nanjing 210093, China
E-mail: kelxl@163.com; xuegi@nju.edu.cn

photon. As shown in Fig. 1, in an SFG experiment, a visible beam with a fixed frequency and an infrared beam with a tunable frequency temporally and spatially overlapped at a surface or an interface. Besides the two naturally reflected beams with respect to the input visible and infrared beams, a third reflected beam (SFG signal) with its frequency being the sum of the visible and infrared frequencies may also be generated, especially when the input infrared frequency is tuned over a vibrational resonance of the surface/interfacial molecules. SFG signal is contributed by molecules on surfaces/at interfaces, due to the selection rule of the SFG process, which will be discussed further below. An SFG spectrum is obtained by plotting the intensity of the SFG signal beam versus the input infrared frequency, which is a vibrational spectrum like an infrared absorption spectrum.

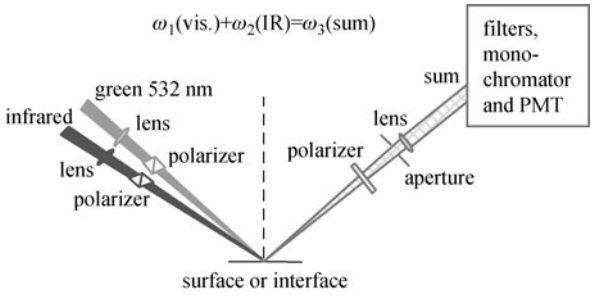

Figure 1 A schematic SFG sample geometry

2.1 Theory

Interaction of photon(s) with a molecule can induce a dipole moment with different orders, depending on the number of photon(s) interacting with the molecule [27]. The induced dipole moment can be written as an expanded power series, as shown in Eq. (1) [27]. The first term in each order in this polynomial defines the polarizability of each order, describing the relationship between the corresponding induced dipole moment and the interacting photon(s). Sequentially, the first order, second order, and third order polarizability…, are defined. In this equation, SFG corresponds to the second item and is a second-order nonlinear optical process.

$$\vec{\mu}_{in} = \alpha_{ij} \cdot \vec{E} + \beta_{ijk} : \vec{E}_1\vec{E}_2 + \gamma_{ijkl} : \vec{E}_1\vec{E}_2\vec{E}_3 + \cdots. \quad (1)$$

When SFG is used to detect the molecular vibration, it is easy to use a schematic energy level diagram to describe this process, as shown in Fig. 2. When a resonance is reached in an SFG process, a photon in the infrared frequency range (ω_1) matching the vibrational transition energy brings the vibration from the ground state to the first excited state. Another photon in the visible frequency range (ω_2) then continues to pump the molecule to a virtual electronic state. The molecule coming back from the virtual electronic state to the ground state generates a third photon in the visible range, with the energy conservation ($\omega = \omega_1 + \omega_2$). It can be recognized immediately from Fig. 2 that an SFG process can be regarded as a combination of an infrared absorption process and an anti-stokes Raman scattering process. Therefore, it is easy to understand that the SFG hyperpolarizability (a second-order polarizability) can be written as the product of the infrared transition dipole moment and Raman polarizablity with respect to the normal coordinate of the vibration, as shown in Eq. (2) [28], where ε_0 is the surrounding medium dielectric constant; ω_q is the angular frequency of the qth vibrational mode.

$$\beta_{ijk} = -\frac{1}{2\varepsilon_0\omega_q}\frac{\partial\alpha_{ij}}{\partial Q_q}\frac{\partial\mu_k}{\partial Q_q}. \quad (2)$$

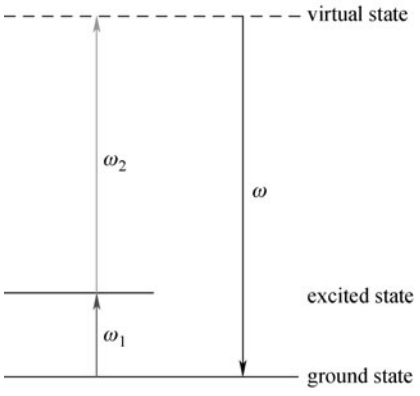

Figure 2 A schematic energy level diagram for an SFG process

In the macroscopic scale or from the experimental viewpoint, it should be noted that, SFG can only detect a collection of hyperpolarizabilities of a large number of molecules on surfaces or at interfaces, which is called the second-order nonlinear optical susceptibility ($\chi^{(2)}_{ijk}$), as shown in Eq. (3) [11,27], where N_s is the number density of molecules in the detected surface/interfacial area and the bracket indicates an average over all orientations of the molecules. The collection of the induced dipole moments is called "polarization", as shown in Eq. (4) [11,27].

$$\chi^{(2)}_{ijk} = N_s\langle\beta_{ijk}\rangle, \quad (3)$$

$$\vec{P}_{in} = \chi^{(2)}_{ijk} : \vec{E}_1\vec{E}_2. \quad (4)$$

It is vitally important that, $\chi^{(2)}_{ijk}$ is a polar tensor, which means that it changes sign under an inversion operation. In a centro-symmetric medium, nothing should change under an inversion operation. This indicates that $\chi^{(2)}_{ijk}$ for a medium with

inversion symmetry has to be zero to satisfy both the conditions described above, as shown in Eq. (5). Most bulk materials posses inversion symmetry, therefore SFG signal, which is proportional to the square of $\chi^{(2)}_{ijk}$, is vanished. $\chi^{(2)}_{ijk}$ can survive at a surface or an interface where the inversion symmetry is broken, as presented in Eq. (6). Therefore for many materials, SFG is intrinsically a surface and interface sensitive technique. This differentiates it from other surface sensitive spectroscopic techniques like ATR-IR, XPS, and SIMS, etc., where the penetration depth of the input or output photons/particles determines the surface specificity.

$$\chi^{(2)}_{ijk}(\text{centrosymmetric}) = 0, \tag{5}$$

$$\chi^{(2)}_{ijk}(\text{surface/interface}) \neq 0. \tag{6}$$

2.2 Data analysis

The SFG output intensity has been derived in the reflection geometry as shown in Eq. (7) [27,28], where $n_i(\omega_i)$ is the refractive index of the incident medium at frequency ω_i, ω and β are the frequency and the reflection angle of the output beam, respectively. β can be deduced based on the moment conservation of the input and output photons. $I_1(\omega_1)$ and $I_2(\omega_2)$ are the intensities of the two input fields with frequencies ω_1 and ω_2. T is the pulse-width of both input lasers. A is the overlapping cross section of the two input beams at the sample, and $\chi^{(2)}_{\text{eff}}$ is the effective second-order nonlinear optical susceptibility. The different components of $\chi^{(2)}_{\text{eff}}$ can be measured using different polarization combinations of the input and output laser beams in the SFG experiment. For example, $\chi^{(2)}_{\text{eff},ssp}$, $\chi^{(2)}_{\text{eff},sps}$, $\chi^{(2)}_{\text{eff},pss}$, and $\chi^{(2)}_{\text{eff},ppp}$ are the components of the effective second-order nonlinear susceptibility measured in the experiment by collecting the *ssp* (*s*-polarized sum frequency signal, *s*-polarized visible input, and *p*-polarized IR input), *sps*, *pss*, and *ppp* SFG spectra.

$$I(\omega) = \frac{8\pi^3\omega^2\sec^2\beta}{c^3 n_1(\omega_1)n_1(\omega_2)n_1(\omega)}|\chi^{(2)}_{\text{eff}}|I_1(\omega_1)I_2(\omega_2)AT. \tag{7}$$

The effective second-order nonlinear optical susceptibility $\chi^{(2)}_{\text{eff}}$ can be related to the second-order nonlinear optical susceptibility defined in the laboratory fixed coordinate (*xyz*) system. Normally, *z* is defined as along the surface normal, while *xz* is the plane containing the input and output laser beams. Therefore we have:

$$\chi^{(2)}_{\text{eff},ssp} = L_{yy}(\omega)L_{yy}(\omega_1)L_{zz}(\omega_2)\sin\beta_2\chi_{yyz}, \tag{8a}$$

$$\chi^{(2)}_{\text{eff},sps} = L_{yy}(\omega)L_{zz}(\omega_1)L_{yy}(\omega_2)\sin\beta_1\chi_{yzy}, \tag{8b}$$

$$\chi^{(2)}_{\text{eff},pss} = L_{zz}(\omega)L_{yy}(\omega_1)L_{yy}(\omega_2)\sin\beta\chi_{zyy}, \tag{8c}$$

$$\begin{aligned}\chi^{(2)}_{\text{eff},ppp} = &-L_{xx}(\omega)L_{xx}(\omega_1)L_{zz}(\omega_2)\cos\beta\cos\beta_1\sin\beta_2\chi_{xxz}\\ &-L_{xx}(\omega)L_{zz}(\omega_1)L_{xx}(\omega_2)\cos\beta\sin\beta_1\cos\beta_2\chi_{xzx}\\ &+L_{zz}(\omega)L_{xx}(\omega_1)L_{xx}(\omega_2)\sin\beta\cos\beta_1\cos\beta_2\chi_{zxx}\\ &+L_{zz}(\omega)L_{zz}(\omega_1)L_{zz}(\omega_2)\sin\beta\sin\beta_1\sin\beta_2\chi_{zzz}.\end{aligned} \tag{8d}$$

In Eqs. (8)a-d, χ_{yyz}, χ_{yzy}, χ_{zyy}, χ_{xxz}, χ_{xzx}, χ_{zxx}, and χ_{zzz} are different susceptibility components in the laboratory coordinate system. L_{ii}'s (i = x, y, or z) are the Fresnel coefficients, and β, β_1, and β_2 are the angles between the surface normal and the output sum beam, the input visible beam, and the input IR beam, respectively.

The Fresnel coefficients (*Lii*'s) of a surface or interface sandwiched between two media have been given in the SFG reflection geometry, as shown in Eqs. (9)a-c [28]. Here $n'(\omega)$ is the refractive index of the interfacial layer, β is the beam incidence angle, and γ is the refracted angle. These three equations work for both the input and output beams.

$$L_{xx}(\omega) = \frac{2n_1(\omega)\cos\gamma}{n_1(\omega)\cos\gamma + n_2(\omega)\cos\beta}, \tag{9a}$$

$$L_{yy}(\omega) = \frac{2n_1(\omega)\cos\beta}{n_1(\omega)\cos\beta + n_2(\omega)\cos\gamma}, \tag{9b}$$

$$L_{zz}(\omega) = \frac{2n_2(\omega)\cos\beta}{n_1(\omega)\cos\gamma + n_2(\omega)\cos\beta}\cdot\left(\frac{n_1(\omega)}{n'(\omega)}\right)^2. \tag{9c}$$

$\chi^{(2)}_{ijk}$ ($i, j, k = x, y, z$) is actually a tensor with 27 components and is the sum of all the hyperpolarizabilities of the molecules probed in the SFG experiment. As discussed above, hyperpolarizability is defined in the molecular coordinate system. Transformation from the molecular hyperpolarizability to the second-order nonlinear susceptibility can be carried out by the transformation from the molecule-fixed coordinate system to the laboratory-fixed coordinate system. Here we discuss this transformation, using a para-substituted phenyl ring as an example, as shown in Fig. 3. The para-substituted phenyl ring belongs to C_{2v} symmetry. The molecule-fixed coordinate system is defined as (*a*, *b*, *c*) system (left graph in Fig. 3). *c* axis is in the same direction as the main axis; *a* axis is in the direction perpendicular to *c* axis and inside the phenyl plane; *b* axis is in the direction perpendicular to the phenyl plane. As shown above, the laboratory-fixed coordinate system is defined as (*x*, *y*, *z*) system. Euler angles (ψ, θ, ϕ) are usually used to describe the relationship between the (*a*, *b*,

c) system and the (*x*, *y*, *z*) system (right graph in Fig. 3). ψ is defined as the rotation angle of the phenyl ring with respect to *z* axis (also called azimuthal angle); θ is the angle between the surface normal and *c* axis (also called tilt angle); ϕ is the rotation angle of the phenyl ring with respect to its main axis *c* (also called twist angle). With the defined Euler angles, Hirose et al. derived the transformation explicitly expressing the laboratory-fixed susceptibility tensor components in terms of the molecule-fixed tensor components, which facilitates the SFG data analysis by avoiding the lengthy calculation of the coordinate transformation [29].

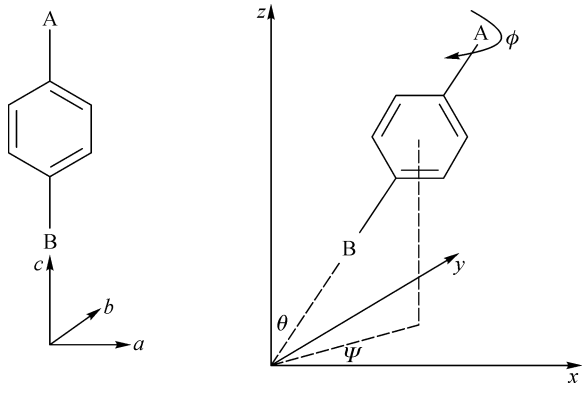

Figure 3 A para-substituted phenyl group in a molecule-fixed coordinate (*a*, *b*, *c*) system (left) and surface/interface-fixed coordinate (*x*, *y*, *z*) system (right). Euler angles (ψ, θ, ϕ) are defined for the coordinate transformation between two systems, which facilitates the description of the orientation of the functional groups on a surface or at an interface.

The surface or interface is normally an azimuthal isotropic plane. Therefore, there are only four independent nonzero second-order nonlinear susceptibility tensor components, as shown in Eqs. (10) [30].

$$\chi_{xxz} = \chi_{yyz}, \chi_{xzx} = \chi_{yzy}, \chi_{zxx} = \chi_{zyy}, \chi_{zzz}. \tag{10}$$

To avoid the calibration of the absolute SFG output intensity (Eq. (7)) in the spectral analysis, people usually collect SFG spectra with different polarization combination(s). With the help of the coordinate transformation, the ratios between different $\chi^{(2)}$ tensors can be written as a function of Euler angles. By solving such equations, Euler angles can be acquired and thus used to characterize the molecular orientation at the surfaces or interfaces. Because a large number of molecules cannot adopt the same orientation at a specific surface or interface, a distribution function is a better representation instead of a single group of Euler angles. A Gaussian function distribution has been generally accepted to approximate the real angle distribution [31,32]; for example, a Gaussian expression of a trigonometric function "cosθ" can be written in a form as shown in Eq. (11)a and b.

$$f(\theta) = C\exp\left[-\frac{(\theta-\theta_0)^2}{2\sigma^2}\right], \tag{11a}$$

$$\langle\cos\theta\rangle = \int \cos\theta f(\theta)\sin\theta \mathrm{d}\theta, \tag{11b}$$

where *C* is a normalization constant and σ is the root-mean-square width.

Mathematically, SFG spectra can be fitted using the following equation:

$$\chi^{(2)}_{ijk} = \chi_{\mathrm{NR}} + \sum_q \frac{A_q}{\omega_2 - \omega_q + i\Gamma_q}. \tag{12}$$

The χ_{NR} term is called the non-resonant background. It is normally a constant item without changing as a function of the scanned infrared frequency. However, χ_{NR} has substantial effect on the line shape of generated SFG spectra depending on the phase difference between χ_{NR} and resonant SFG signals [33]. Somehow χ_{NR} is quite useful in that it provides a reference helping determine the absolute orientation of the detected functional groups especially when a large nonresonant background exists [34,35]. A_q, ω_q, and Γ_q are the strength, resonant frequency, and damping coefficient of the vibrational mode q.

3 Application of SFG in polymer science

Many polymer materials have a large number of flexible long chains, which are widely used in different applications ranging from advanced technology to daily life. For example, polymers can be used as construction materials, templates for nanofabrication, drug carriers, marine anti-biofouling coatings, and encapsulating materials in microelectronic devices [36–40]. In many of these applications, polymer surface or interfacial properties like adhesion, wettability, lubrication, and friction, etc., are crucial. As mentioned above, polymer surface/interfacial properties are determined by their surface/interfacial structures. The SFG vibrational spectroscopy with the submonolayer sensitivity is an ideal technique to characterize the molecular level structural information of polymer surfaces and interfaces, which can be correlated to the macroscopic surface and/or interfacial properties.

3.1 Polymer surfaces in air and surface restructuring upon contacting liquids

The first study of using SFG to examine a polymer surface and to detect surface restructuring in water was to investigate a polyurethane-type polymer with polydimethylsiloxane

(PDMS) end groups by Somorjai group [41]. It was found that in air the hydrophobic PDMS end groups covered most of the surface area. When immersed in water, the polymer surface underwent an obvious restructuring with the hydrophobic PDMS part gradually retreating from the surface and the hydrophilic polyurethane part gradually moving to the surface. This surface restructuring was reversible although the restructuring time scales from air to water (25 h) and from water to air (3 h) are different. This research leads to an important conclusion that the characterization of the polymer surfaces in the working environments is important in order to properly describe the surface properties. The polyethylene and polypropylene surface structures were then explored by the same group [42] and it was found that the methoxy resonant signals dominated the SFG spectra in commercial PE and PP samples, indicating that the additives segregated from the bulk to the polymer surfaces. This finding is important at the technological level because it proves that SFG can help determine the surface compositions of commercial polymers and the surface segregation of the additives.

The surface restructuring behavior of a cross-linked polymer, poly (2-hydroxyethyl) methacrylate (PHEMA) was studied by Somorjai group later [43]. They found that the SFG spectrum of the PHEMA surface in air was dominated by the methyl symmetric stretching mode while the methylene symmetric stretching mode from the side ethylene glycol groups appeared after contacting the surface to water. Based on this spectral difference, they suggested that PHEMA can have a hydrophobic conformation or hydrophilic conformation on the surface depending on the contacting medium.

Shen group systematically studied the surface structure of polyvinyl alcohol (PVA). This polymer is widely used in the liquid crystal (LC) display industry as substrates to obtain the top LC bulk alignment upon rubbing [31,44]. In this research, a comprehensive orientation analysis of backbone methylene groups on the PVA surface was presented and all of the three methylene orientation angles were deduced. It was found that rubbing can lead to the surface PVA backbones aligning well in the rubbing direction, which is the reason for the top homogeneous alignment of LC films. The similar rubbing induced surface ordering phenomena were also studied for the poly(vinyl cinnamate) [45,46] and polyimide surfaces [47,48].

The surface structures and restructuring behaviors in water of polymethacrylates with different side chains were systematically investigated by Chen group [49–52]. It was discovered that the polymethylmethacrylate (PMMA) surface in air was dominated by the ester methyl groups with more or less a normal orientation to the surface, with a tilt angle between two extremes of 33° supposing a δ-distribution and 0° with a distribution width of 31° assuming a Gaussian distribution [49]. No substantial structural change of the PMMA surface in water was observed. The SFG spectral intensity difference of the PMMA surface in air and in water were attributed to the refractive index difference of the air and the water; the spectra of the PMMA surface in air and in water after normalized by Fresnel coefficients were similar in features and intensities [50]. When the side chain length increases, as polybutylmethacrylate (PBMA) and polyethylmethacrylate (PEMA), substantial SFG spectral change in water (compared to that in air) was observed, indicated by different symmetric and asymmetric stretching signal intensities. Detailed analysis suggested that the side chain end methyl groups "standed up" with a broad tilt angle distribution in air and "lay down" with a narrow tilt angle distribution in water on the surface [50–53]. When the side chain length further increases, as poly(n-octylmethacrylate) (POMA) and poly(n-octadecylmethacrylate) (PODMA), spectral differences in water were also observed [50]. Interestingly, except for POMA, all the other polymethacrylates showed reversible structural changes in water as evidenced by the recovery of the SFG spectra after the samples exposing to air from water again [50,53]. The chain rigidity as a function of the side chain length was believed to be the reason for the observation. PMMA is a rigid polymer and the ester methyl groups of PMMA are more hydrophilic than the normal methyl groups of other polymethacrylates. Such ester methyl groups did not need to change the orientation when contacting water to adapt to the hydrophilic environment. The unfavorable interactions between the normal methyl groups of other polymethacrylates on the surface and water molecules drove the normal methyl groups to orient more toward the surface. As the side chain length increases, the chain rigidity decreases and the backbone reorientation occurs. Therefore the irreversible surface restructuring was observed for POMA. As the side chain length further increases, the high backbone mobility makes the backbone relaxation fast enough in a time scale through which the intermediate relaxation cannot be sensed by SFG (PODMA) and only the surface structure in air and water of fully relaxed states can be detected [53].

The polymer/silane interfacial ordering was also systematically examined by Chen and Loch et al. using SFG [54–56]. Depending on the chemical structures of polymers and silanes (head, backbone, and end groups), the silane molecules can form different ordered states at the polymer/silane interfaces, from which the molecular mechanism of the polymer adhesion could be elucidated.

The SFG study of polystyrene (PS) surface in air and buried interface with sapphire in total reflection geometry was performed by Dhinojwala group [57]. (For more details, see Section 3.2). The SFG spectra of PS surface in air were found to be dominated by the symmetric C-H vibrational modes of

the phenyl rings. The orientation of the phenyl rings was quantitatively evaluated according to the SFG signals from the v_{7a} and v_{20b} modes and it was found that the phenyl rings were more likely parallel in air (tilt angle around 20°) with respect to the surface normal [57].

Richter and his colleagues examined the PS surface structure in air using PS thin films on oxidized Si substrates [58]. By analyzing the SFG signals contributed by the v_2 and v_{7a} modes in the *ssp* and *sps* spectra, they claimed that the pendant phenyl groups adopted a tilt angle of 57° with a twist angle of 48°. By comparing the PS SFG spectra to those of a self-assembled monolayer of phenylsiloxane, they concluded that the pendant phenyl groups were orientated away from the PS film to achieve the maximum free volume. Also this was possibly due to the lowest free energy conformation that smoothed out the abrupt change in density from the presence of the free surface [58]. It should be noted that the twist angle they obtained (48°) can be hardly differentiated from an isotropic distribution of the twist angle. The tilt angle they obtained (57°) is different from the tilt angle obtained by Dhinojwala group (around 20°) [57]. Such an angle difference may be due to the different substrates used in making PS films or other reasons. Richter and his colleagues also carried out research to selectively probe the free and the buried interfaces of PS thin films on spin-on glass (SOG) substrates [59], based on the dependence of the Fresnel coefficients of the free surface and the buried interface on the film thickness. They discovered that the pendant phenyl group orientation at the buried PS/SOG interface was similar to that of the free surface, with the phenyl groups pointing away from the bulk PS [59].

In addition, Richter et al. studied the restructuring of the PS surface upon exposure to both the low-surface-tension liquids (hexane, methanol, and ethanol) and high-surface-tension liquids (water and glycerol) using SFG [60]. It was observed that the pendant phenyl groups on PS in the low-surface-tension liquids adopt low tilt angles, and in the high-surface-tension liquids adopted a near flat orientation with respect to the PS surface plane [60]. The PS surface restructuring was also studied by Somorjai group under the saturated toluene vapor environment [61]. The surface order of pendant phenyl groups disappeared after exposing the PS surface to the toluene vapor, and recovered after removing the surface from the vapor. It was believed that the toluene vapor can solvate the PS surface and thus destroy the surface order; and the partially solvated PS surface can easily recover because of its high mobility [61].

When the polymers are hydrophilic, the hydrogen bonding may play an important role for the surface restructuring. Ye et al. studied the surface carbonyl stretching mode of a biocompatible polymer, poly(2-methoxyethyl acrylate) (PMEA) upon contacting water and bisphenol A using SFG [62]. Three different surface states based on positions of the SFG peak centers were suggested. The three peak centers were attributed to the free carbonyl groups at 1740 cm^{-1}, carbonyl groups hydrogen-bonded to water at 1722 cm^{-1}, and carbonyl groups hydrogen-bonded to bisphenol A at 1715 cm^{-1}, respectively. The reversible surface restructuring behavior of a biphenyl type phenol resin (BPP) exposed to humid air was examined by Chen group [63]. Two main SFG spectral feature changes were observed. One was the increased signal from the v_2 mode (or total symmetric stretching mode) at 3063 cm^{-1} for the *ssp* spectra after exposing to humid air (or water adsorption). The other was a red shift of the hydroxyl vibration from 3540 cm^{-1} to 3520 cm^{-1}. These spectral changes were explained by the formation of hydrogen bonds between the phenol groups and water molecules adsorbed on top of the BPP resin, causing the surface phenol groups to adopt a "perpendicular-like" orientation.

Wang and his colleagues studied the surface strucutures of random copolymers composed of methacrylates and fluorinated units solidified from the solution using SFG and other techniques [64–66]. It was found that: when the fluorinated unit content was low, the entropic force may dominate the surface structure since the random coil conformation in the solution can greatly affect the final conformation of the copolymer chains at the surface; when the fluorinated unit content was high, the enthalpic force may dominate the surface structure since the fluorinated moieties were prone to segregate to the surface [64]. Besides, the effects of different solvents and the film-forming methods were also discussed [65,66].

3.2 Polymer/Solid interfaces

The polymer/solid interface was first probed by Dhinojwala group using a total internal reflection geometry [57]. The high refractive index sapphire prism was used in their study with a relatively low refractive index polystyrene film deposited on one side of the prism so that the total internal reflection can happen at the sapphire prism/PS interface. As shown in Fig. 4, by selecting the appropriate incident angles for the visible and infrared beams, the PS vibrational signal at the sapphire/PS interface (incident angles near 64°) as well as the PS surface signal in air (incident angles near 36°) can be detected separately. In their case, changing the incident angles led to the change of the relative Fresnel coefficients between the PS surface in air and the PS/sapphire interface so that the selective detection of the surface or buried interface was feasible. It was found that both the *ssp* and *ppp* SFG spectra at the sapphire/PS interface were dominated by the phenyl C-H

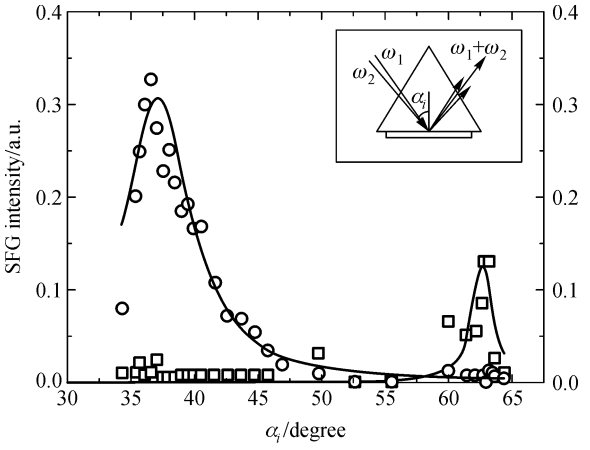

Figure 4 The SFG intensity Issp as a function of incident angle α_i for two wave numbers (ω_2), 3027 cm^{-1} (squares) and 3067 cm^{-1} (circles). The data represented by circles are scaled by a factor of 5. The solid line is a visual guide to illustrate the spectral trends. (Reproduced with permission from Phys. Rev. Lett. 85: 3854–3857 (2000). Copyright 2000 American Physical Society)

stretching vibrational modes instead of the methylene stretching vibrational modes. Using the signals contributed by the v_{20b} and v_{7a} modes, they found that the phenyl groups at the sapphire/PS interface nearly lay down [57]. The two interfaces between the PS and poly(vinyl n-octadecyl carbamate-co-vinyl acetate) (PVNODC) and between the PS and poly(octadecyl acrylate) (PA-18) using the same total internal reflection geometry were then studied [67,68]. At both interfaces, the observed strong methylene SFG signals suggested the presence of gauche defects in the side alkyl chains. The orientation of methyl groups at the PS/PVNODC interface was found to be similar to that on the PVNODC surface in air, i.e., adopting a low-tilt-angle orientation. They also found that the phenyl groups at both the PS/PVNODC and PS/PA-18 interfaces adopted a similar orientation as the PS/sapphire interface, i.e., adopting a high-tilt-angle orientation [67]. In-depth studies on the understanding of the molecular structures of buried interfaces upon interfacial motion were also carried out by Dhinojwala and his colleagues. The two interfaces between PDMS and PS, and between PDMS and PVNODC were probed under external pressure using SFG [69]. It was found that the friction force between PDMS and PS was a factor of 4, higher than that between PDMS and PVNODC. The difference of the friction force was explained according to the difference of the interfacial structures under pressure [69]. In the case of PDMS/PS interface under pressure, PDMS and PS chains at the interface interpenetrated, which was sensed by SFG, and a high friction force was measured by a mechanic sensor. In the case of PDMS/PVNODC interface, the PVNODC side chain crystallization prevented interfacial restructuring, which was also detected by SFG, and a low friction force was measured by a mechanic sensor. In another paper discussing the adhesion between PDMS and the sapphire substrate in the presence of water, Dhinojwala group found that the friction coefficient (defined as the shear force/normal force) was much larger than that estimated from a model assuming the existence of a uniform water layer between PDMS and the sapphire substrate [70]. By detecting the interfacial molecular structures using SFG, they concluded that the PDMS/sapphire interface was heterogeneous with two distinct regions: one was the region where the PDMS chains were directly in contact with the surface hydroxyl groups on the sapphire substrate as evidenced by an SFG peak at 3690 cm^{-1}, the other was the region where a thin layer of water (many layers of water molecules) was trapped between PDMS and the sapphire substrate; and the first region was responsible for the observed high friction coefficient [67].

Somorjai group studied the PMMA/sapphire and PBMA/sapphire interfacial structures under pressure using SFG [71]. The SFG spectrum of the PMMA/sapphire interface was dominated by the signal from the ester methyl symmetric stretching mode; when pressure was applied, there was no substantial spectral change. The SFG spectrum of the PBMA/sapphire interface was dominated by the signal from the end group methyl symmetric stretching mode; but when pressure was applied, there was substantial spectral change observed, indicating that the interfacial restructuring did occur. Somorjai et al. attributed the different interfacial restructuring behaviors of the PMMA/sapphire and PBMA/sapphire interfaces to the different chain mobilities at the room temperature. At the room temperature PBMA (T_g= 15°C) is in the rubbery state so that the high chain mobility was the reason for the observed PBMA interfacial restructuring. At the room temperature PMMA (T_g= 105°C) is in the glassy state so that it is difficult for the interfacial restructuring to happen [71].

The polymer/metal interfacial structures were probed using SFG by Chen group [35,72]. Considering the SFG resonant signals generated from both the interfaces for a PMMA film on a silver (Ag) substrate, deconvolution of the PMMA/air and PMMA/Ag interfacial signals can be done by including the Fresnel coefficients of the two interfaces into the spectral fitting and analysis for PMMA films with varied thicknesses [72]. It was found that the ester methyl groups of PMMA at the PMMA/Ag interface tilted more from the surface normal compared to those at the PMMA/air interface. An SFG experimental geometry by sandwiching a polymethylacryalte (PMA) thin film between a fused silica and a Ag substrate was then developed [35]. The advantage for this experimental geometry is that the hydrophilic nature of the silica surface can suppress the order of the hydrophobic ester methyl groups at the PMA/silica interface, leading to no detectable SFG

signal from this interface. As a result, the molecular order of the ester methyl groups at the PMA/Ag interface can be directly probed without considering the interference from the PMA/silica interface. Besides, by comparing the phase difference between the resonant ester methyl symmetric stretching signal and the nonresonant background for the PMA/Ag interface and a SAM of methyl 3-mercaptopropionate on Ag surface, the absolute orientation of the ester methyl groups at the PMA/Ag interface was deduced: They tilt away from the Ag surface.

3.3 Surface and interface dynamics

The study of the dynamic behavior of the polymer surfaces at different temperatures using SFG was first performed by Somorjai and Shen et al. [73]. By comparing the SFG intensity ratio of methylene and methyl symmetric stretching modes as a functional of environmental temperature, the surface glass transition temperatures (T_gs) of atactic polypropylene (APP) and isotactic polypropylene (IPP) were determined, which were the same as the bulk T_gs of APP and IPP [73]. Shen group measured the surface T_g of PVA in air by using SFG to monitor the temperature-dependent spectral change from the rubbing-induced azimuthal anisotropy to isotropy [74]. It was found that the surface relaxation of PVA was two-dimensional, parallel to the surface, and the obtained T_g ((58±2)°C) was essentially the same as that of the bulk PVA detected by DSC ((59±1)°C). Shen et al. believed that the rubbing induced PVA surface was composed of aligned PVA chains which cannot relax before the underlying chains in the bulk start to relax [74].

Somorjai group also studied the segregation of polymer blends consisting of atactic polypropylene (aPP) and aspecific poly(ethylene-co-propylene) rubber (aEPR) at the hydrophilic solid sapphire and hydrophobic air interfaces. The preferential segregation of aPP component at both the interfaces after annealing was detected by SFG [75]. The driving force to promote the segregation at both the interfaces was aPP's high conformational entropy resulting from its relatively short segmental length.

The surface and interface transition temperatures of the alkyl-side chain-acrylate comb (poly[vinyl n-octadecyl carbamateco-vinyl acetate], PVNODC) polymers in air and with the sapphire interface respectively were measured by Dhinojwala group [67,68,76]. Two transitions at the polymer surface in air and one transition at the polymer/sapphire interface were observed based on the dominate peak intensity (methyl at the polymer surface in air and methylene at the polymer/sapphire interface) change as a function of temperature. Based on their experiment, a stable intermediate smectic-like surface ordered state above the bulk transition temperature in air was proposed, which was believed to be stabilized by the surface free energy [67,68]. Dhinojwala group then used SFG to study the water contact angle hysteresis of the same polymer (PVNODC) and the self-assembled monolayer (SAM) of octadecyltrichlorosilane (OTS) as a comparison [76]. The SFG spectra of the PVNODC surface in air were dominated by the side chain methyl vibrations, and when the PVNODC surface was in contact with water, the side chain methylene vibrations appeared and the intensity of the side chain methyl vibrations did not change. For both the OTS/air and OTS/water interfaces, the SFG spectra were dominated by the side chain methyl vibrations. Based on this, Dhinojwala et al. suggested that the PVNODC surface was heterogeneous with crystalline domains of side chains enclosed by less ordered, grain-boundary regions. When the PVNODC surface was exposed to water, the surface restructuring occurred in the less-ordered regions, which was the reason for the appearance of the methylene vibrations in the SFG spectra and the contact angle hysteresis; while the OTS surface was covered by a homogeneous crystalline SAM layer, the surface restructuring cannot happen and the surface contact angle hysteresis was thought due to the surface roughness effect, supported by the AFM characterization [76].

To study the interfacial motion between the PS and alkanes, Dhinojwala group used SFG to detect the SFG intensity change of the ν_2 mode of the PS phenyl groups and the symmetric stretching mode of the alkane methyl groups as a function of temperature [77]. Based on the temperature dependent intensity change, it was found that the PS interfacial motion was coupled with the alkane transition temperature and decoupled from the bulk T_g of PS. The possible reason was that the observed transitions were due to the sub-T_g motions or the faster segmental relaxations on the PS surface. No matter which reason (sub-T_g motions or faster segmental relaxation) was correct, the strong coupling between the interfacial motions of PS and alkanes confirmed that the interfacial interaction can play an important role in determining the polymer interfacial dynamics. Another study by Dhinojwala group using hexadecanol also proved that the interfacial interaction can have a substantial or even a decisive effect on the dynamics and the resulting structure at the interfaces [78].

In examining the dependence of the shear stress between the cross-linked PDMS lens and the glassy polyacrylates on the aging time, Dhinojwala group found that XPS and contact angle measurement cannot give the explainable information, but SFG revealed the interfacial structural difference upon applying the shear stress [79]. When a shear stress was applied, a dramatically increased methyl symmetric vibration peak of PDMS at 2910 cm^{-1} was observed with the aging time increasing. A model was proposed to explain the aging effect

on the surface structure of PDMS. It was believed that aging can result in PDMS chain scission and produce the dangling PDMS chain tethered with one end chemically attached to the cross-linked PDMS network and the other end free on the surface; these tethered PDMS chains on the surface can easily be aligned into a well ordered state under the external mechanic shear [79]. This model explained why the side methyl groups of the aged PDMS surface were highly ordered upon the application of a shear stress, demonstrating that the polymer surface dynamics as well as the surface structure can easily be changed on account of prolonged aging or exposure to air by accumulated minor chemical process.

Chou and his colleagues studied the surface structure relaxation of PMMA [80]. Two surface transition temperatures were observed at 107°C and 67°C respectively. They believed the first transition (107°C) was the bulk-induced structure relaxation since it agreed well with the bulk T_g of PMMA. They proposed that the second transition (67°C) might come from either the surface T_g (α-relaxation) or β-relaxation since the detected signal comes from the side chain ester methyl groups [80].

4 Summary

SFG is a novel second-order nonlinear vibrational spectroscopy with excellent surface/interface specificity and molecular orientation sensitivity. It is a unique technique which can provide in situ molecular information regarding surface and interfacial structures, helping to elucidate the structure-property relationships in extensive research areas associated with surface and interfacial sciences. Here we discussed its power and success in studying polymer surfaces in air, polymer surface restructuring in different chemical environments, buried polymer-solid interfaces, and polymer surface and interfacial dynamics. There are several other important SFG research directions related to polymer science which are not covered in this review paper, including biomedical polymers, biologic polymers, and conductive polymers. For these systems, SFG was also demonstrated to be an important analytical probe to advance our understanding on the structural origins of their surface or interfacial properties at the molecular level. The prediction that "the mature years of Sum-Frequency Generation are ahead" [81] is becoming true.

Acknowledgements This work was supported by the Zhejiang Provincial Natural Science Foundation of China (Y4100390), the start-up fund of Zhejiang Sci-Tech University (0913845-Y), the funds from the Key Laboratory of Advanced Textile Materials and Manufacturing Technology of Education Ministry, Zhejiang Sci-Tech University (2009QN07) and the Department of Education of Zhejiang Province (Y200909780). We also acknowledge the financial supports from the National Natural Science Foundation of China (NSFC, Nos. 20704038 and 20874089), the Program for Changjiang Scholars and Innovative Research Team in University (No. IRT 0654).

References

1. Harrick, N. J., *Internal Reflection Spectroscopy*; John Wiley & Sons: New York, **1967**
2. Tamm, L. K.; Tatulian, S. A., *Q. Rev. Biophys*. **1997**, *30*, 365–429
3. Moskovits, M., *Rev. Mod. Phys*. **1985**, *57*, 783–826
4. Metiu, H.; Das, P., *Annu. Rev. Phys. Chem*. **1984**, *35*, 507–536
5. Fadley, C. S., *Prog. Surf. Sci*. **1984**, *16*, 275–388
6. Somorjai, G. A., *Chem. Rev*. **1996**, *96*, 1223–1236
7. Shonaike, G. O.; Simon, G. P., eds., *Polymer Alloys and Blends*; Marcel Dekker: New York, **1999**
8. Fischer, D. A.; Efimenko, K.; Bhat, R. R.; Sambasivan, S.; Genzer, J., *Macromol. Rapid Commun*. **2004**, *25*, 141–149
9. Hähner, G., *Chem Soc Rev* **2006**, *35*, 1244–1255
10. Hunt, J. H.; Guyot-Sionnest, P.; Shen, Y. R., *Chem. Phys. Lett*. **1987**, *133*, 189–192
11. Shen, Y. R., *Nature* **1989**, *337*, 519–525
12. Hirose, C.; Akamatsu, N.; Domen, K., *Appl. Spectrosc*. **1992**, *46*, 1051–1072
13. Eisenthal, K. B., *Chem. Rev*. **1996**, *96*, 1343–1360
14. Shen, Y. R., *Proc. Natl. Acad. Sci. U.S.A*. **1996**, *93*, 12104–12111
15. Conboy, J. C.; Messmer, M. C.; Walker, R. A.; Richmond, G. L., *Prog. Colloid Polym. Sci*. **1997**, *103*, 10–20
16. Buck, M.; Himmelhaus, M., *J. Vac. Sci. Technol. A* **2001**, *19*, 2717–2736
17. Shen, Y. R., *Pure Appl. Chem*. **2001**, *73*, 1589–1598
18. Chen, Z.; Shen, Y. R.; Somorjai, G. A., *Annu. Rev. Phys. Chem*. **2002**, *53*, 437–465
19. Williams, C. T.; Beattie, D. A., *Surf. Sci*. **2002**, *500*, 545–576
20. Richmond, G. L., *Chem. Rev*. **2002**, *102*, 2693–2724
21. Wang, H. F.; Gan, W.; Lu, R.; Rao, Y.; Wu, B. H., *Int. Rev. Phys. Chem*. **2005**, *24*, 191–256
22. Vidal, F.; Tadjeddine, A., *Rep. Prog. Phys*. **2005**, *68*, 1095–1127
23. Shen, Y. R.; Ostroverkhov, V., *Chem. Rev*. **2006**, *106*, 1140–1154
24. Zheng, D. S.; Wang, Y.; Liu, A. A.; Wang, H. F., *Int. Rev. Phys. Chem*. **2008**, *27*, 629–664
25. Allen, H. C.; Casillas-Ituarte, N. N.; Sierra-Hernández, M. R.; Chen, X.; Tang, C. Y., *Phys. Chem. Chem. Phys*. **2009**, *11*, 5538–5549
26. Geiger, F. M., *Annu. Rev. Phys. Chem*. **2009**, *60*, 61–83
27. Shen, Y. R., *The Principles of Nonlinear Optics*; Wiley: New York, 1984
28. Zhuang, X.; Miranda, P. B.; Kim, D.; Shen, Y. R., *Phys. Rev. B*

1999, *59*, 12632–12640
29. Hirose, C.; Akamatsu, N.; Domen, K., *Appl. Spectrosc*. **1992**, *46*, 1051–1072
30. Guyot-Sionnest, P.; Hunt, J. H.; Shen, Y. R., *Phys. Rev. Lett*. **1987**, *59*, 1597–1600
31. Wei, X.; Zhuang, X.; Hong, S. C.; Goto, T.; Shen, Y. R., *Phys. Rev. Lett*. **1999**, *82*, 4256–4259
32. Simpson, G. J.; Rowlen, L. K., *J. Am. Chem. Soc*. **1999**, *121*, 2635–2636
33. Miranda, P. B.; Shen, Y. R., *J. Phys. Chem. B* **1999**, *103*, 3292–3307
34. Ward, R. N.; Davies, P. B.; Bain, C. D., *J. Phys. Chem*. **1993**, *97*, 7141–7143
35. Lu, X.; Li, D.; Kristalyn, C. B.; Han, J.; Shephard, N.; Rhodes, S.; Xue, G.; Chen, Z., *Macromolecules* **2009**, *42*, 9052–9057
36. Andrade, J. D., ed., *Polymer Surface Dynamics*; Plenum Press: New York, **1988**
37. Park, J. B.; Lakes, R. S., *Biomaterials: an Introduction*; Plenum Press: New York, **1992**
38. Carbassi, F.; Morra, M.; Occhiellp, E., *Polymer Surfaces: From Physics to Technology*; John Wiley and Sons: Chichester, **1994**
39. Rataner, B. D.; Castner, D. G., eds., *Surface Modification of Polymeric Biomaterials*; Plenum Press: New York, **1996**
40. Feast, W. J.; Munro, H. S.; Richards, R. W., eds., *Polymer Surfaces and Interfaces II*; John Wiley and Sons: New York, **1992**
41. Zhang, D.; Ward, R. S.; Shen, Y. R.; Somorjai, G. A., *J. Phys. Chem. B* **1997**, *101*, 9060–9064
42. Zhang, D.; Shen, Y. R.; Somorjai, G. A., *Chem. Phys. Lett*. **1997**, *281*, 394–400
43. Chen, Q.; Zhang, D.; Somorjai, G.; Bertozzi, C. R., *J. Am. Chem. Soc*. **1999**, *121*, 446–447
44. Wei, X.; Hong, S. C.; Zhuang, X.; Goto, T.; Shen, Y. R., *Phys. Rev. E Stat. Phys. Plasmas Fluids Relat. Interdiscip. Topics* **2000**, *62*, 5160–5172
45. Pagliusi, P.; Chen, C. Y.; Shen, Y. R., *J. Chem. Phys*. **2006**, *125*, 201104
46. Jayathilake, H. D.; Zhu, M. H.; Rosenblatt, C.; Bordenyuk, A. N.; Weeraman, C.; Benderskii, A. V., *J. Chem. Phys*. **2006**, *125*, 064706
47. Kim, D.; Oh-e, M.; Shen, Y. R., *Macromolecules* **2001**, *34*, 9125–9129
48. Lee, Y. H.; Seo, J.; Yoon, I.; Park, K.M.; Lee, S. S., *Anal. Sci*. **2001**, *17*, 805–808
49. Wang, J.; Chen, C.; Buck, S. M.; Chen, Z., *J. Phys. Chem. B* **2001**, *105*, 12118–12125
50. Wang, J.; Woodcock, S. E.; Buck, S. M.; Chen, C.; Chen, Z., *J. Am. Chem. Soc*. **2001**, *123*, 9470–9471
51. Wang, J.; Paszti, Z.; Even, M. A.; Chen, Z., *J. Am. Chem. Soc*. **2002**, *124*, 7016–7023
52. Chen, C.; Clarke, M. L.; Wang, J.; Chen, Z., *Phys. Chem. Chem. Phys*. **2005**, *7*, 2357–2363
53. Chen, Z., *Polym. Int*. **2006**, *65*, 577–587
54. Chen, C. Y.; Loch, C. L.; Wang, J.; Chen, Z., *J. Phys. Chem. B* **2003**, *107*, 10440–10445
55. Chen, C. Y.; Wang, J.; Loch, C. L.; Ahn, D.; Chen, Z., *J. Am. Chem. Soc*. **2004**, *126*, 1174–1179
56. Loch, C.; Ahn, D.; Chen, C.; Chen, Z., *J. Adhes*. **2005**, *81*, 319–345
57. Gautam, K. S.; Schwab, A. D.; Dhinojwala, A.; Zhang, D.; Dougal, S. M.; Yeganeh, M. S., *Phys. Rev. Lett*. **2000**, *85*, 3854–3857
58. Briggman, K. A.; Stephenson, J. C.; Wallace, W. E.; Richter, L. J., *J. Phys. Chem. B* **2001**, *105*, 2785–2791
59. Wilson, P. T.; Richter, L. R.; Wallace, W. E.; Briggman, K. A.; Stephenson, J. C., *Chem. Phys. Lett*. **2002**, *363*, 161–168
60. Yang, C. S. C.; Wilson, P. T.; Richter, L. J., *Macromolecules* **2004**, *37*, 7742–7746
61. Opdahl, A.; Somorjai, G. A., *Langmuir* **2002**, *18*, 9409–9412
62. Li, G.; Ye, S.; Morita, S.; Nishida, T.; Osawa, M., *J. Am. Chem. Soc*. **2004**, *126*, 12198–12199
63. Lu, X.; Han, J.; Shephard, N.; Rhodes, S.; Martin, A. D.; Li, D.; Xue, G.; Chen, Z., *J. Phys. Chem. B* **2009**, *113*, 12944–12951
64. Xue, D.; Wang, X.; Ni, H.; Zhang, W.; Xue, G., *Langmuir* **2009**, *25*, 2248–2257
65. Wang, X.; Ni, H.; Xue, D.; Wang, X.; Feng, R. R.; Wang, H. F., *J. Colloid Interface Sci*. **2008**, *321*, 373–383
66. Ye, X.; Zuo, B.; Deng, M.; Hei, Y.; Ni, H.; Lu, X.; Wang, X., *J. Colloid Interface Sci*. **2010**, *349*, 205–214
67. Harp, G. P.; Rangwalla, H.; Yeganeh, M. S.; Dhinojwala, A., *J. Am. Chem. Soc*. **2003**, *125*, 11283–11290
68. Gautam, K. S.; Dhinojwala, A., *Phys. Rev. Lett*. **2002**, *88*, 145501
69. Yurdumakan, B.; Nanjundiah, K.; Dhinojwala, A., *J. Phys. Chem. C* **2007**, *111*, 960–965
70. Nanjundiah, K.; Hsu, P. Y.; Dhinojwala, A., *J. Chem. Phys*. **2009**, *130*, 024702
71. Kweskin, S. J.; Komvopoulos, K.; Somorjai, G. A., *Langmuir* **2005**, *21*, 3647–3652
72. Lu, X.; Shephard, N.; Han, J.; Xue, G.; Chen, Z., *Macromolecules* **2008**, *41*, 8770–8777
73. Gracias, D. H.; Zhang, D.; Lianos, L.; Ibach, W.; Shen, Y. R.; Somorjai, G. A., *Chem. Phys*. **1999**, *245*, 277–284
74. Zhang, C.; Hong, S. C.; Ji, N.; Wang, Y. P.; Wei, K. H.; Shen, Y. R., *Macromolecules* **2003**, *36*, 3303–3306
75. Kweskin, S. J.; Komvopoulos, K.; Somorjai, G. A., *J. Phys. Chem. B* **2005**, *109*, 23415–23418
76. Rangwalla, H.; Schwab, A. D.; Yurdumakan, B.; Yablon, D. G.; Yeganeh, M. S.; Dhinojwala, A., *Langmuir* **2004**, *20*, 8625–8633
77. Harp, G. P.; Rangwalla, H.; Li, G.; Yeganeh, M.; Dhinojwala, A., *Macromolecules* **2006**, *39*, 7464–7466
78. Li, G.; Dhinojwala, A.; Yeganeh, M. S., *J. Phys. Chem. B* **2009**, *113*, 2739–2747
79. Kurian, A.; Prasad, S.; Dhinojwala, A., *Macromolecules* **2010**, *43*, 2438–2443
80. Li, Q.; Hua, R.; Cheah, I. J.; Chou, K. C., *J. Phys. Chem. B* **2008**, *112*, 694–697
81. Guyot-Sionnest, P., *Surf. Sci*. **2005**, *585*, 1–2